IEEE Access
Multidisciplinary | Rapid Review | Open Access Journal

Received 14 October 2022, accepted 19 February 2023, date of publication 28 February 2023, date of current version 8 March 2023.

Digital Object Identifier 10.1109/ACCESS.2023.3250181

RESEARCH ARTICLE

An Improved Parametric Method for Selecting Different Types of Tesla Transformer Primary Coil to Construct an Artificial Lightning Simulator

SUMAN JANA[1], PABITRA KUMAR BISWAS[2], (Member, IEEE), THANIKANTI SUDHAKAR BABU[3], (Senior Member, IEEE), AND HASSAN HAES ALHELOU[4], (Senior Member, IEEE)

[1]Department of Electrical and Electronics Engineering, Regent Education and Research Foundation, Barrackpore, West Bengal 700121, India
[2]Department of Electrical and Electronics Engineering, National Institute of Technology Mizoram, Aizawl, Mizoram 796012, India
[3]Department of Electrical Engineering, Chaitanya Bharathi Institute of Technology (CBIT), Hyderabad 500075, India
[4]Department of Electrical Power Engineering, Faculty of Mechanical and Electrical Engineering, Tishreen University, Lattakia, Syria

Corresponding author: Hassan Haes Alhelou (alhelou@ieee.org)

ABSTRACT Due to the intermittent and hazardous nature of lightning impulse, researchers rely on artificial impulse generators to study it. The Tesla coil is a commonly used device to generate artificial lightning. This paper presents a parametric analysis of the primary side coil of the Tesla transformer. The analysis employs seven key electrical properties: skin depth, current density, voltage distribution, Ohmic loss, electric field strength, charge density, and energy content. These parameters are used to evaluate the response of various coil types to high voltage impulses. The Ansys high-frequency electromagnetic solver is used to perform a comparative analysis of essential parameters. The results can aid lightning researchers and Tesla coil designers in determining the optimal designs for Tesla primary coils in the future. The analyzed data is validated using Tesla coil hardware, which is used as an artificial lightning producer to test the feasibility of a lightning energy harvester.

INDEX TERMS Ansys, flat spiral coil, helical coil, high voltage test, inverse conical coil, impulse generator, lightning energy, Tesla coil.

I. INTRODUCTION

Nature is the mother of all mysteries, and one of the most captivating is lightning. This natural wonder has intrigued humans for centuries, with its power and unpredictability making it a fascinating subject of study. Researchers have been striving to harness its energy for decades. Lightning is a scintillating light flash that occurs when static electricity is suddenly discharged into one or more charged regions in the atmosphere. It can occur within a single cloud, between different clouds, or between the clouds and the atmosphere or ground. As a natural surge, it can be both fascinating and hazardous [1], [2]. The experimental report of Bhattarai and Potapov also agreed that lightning strokes might have a kA range of current magnitude. They also claimed that a single stroke might deliver 250kWh energy and 30kA current [3], [4]. Hasbrouck, Rakov, and later Cao explored and reported that insulation breakdown of air ensues approximately at 5MV. They also have confirmed that a lightning bolt conveys almost 30 kA current with almost 150kWh energy on average [5], [6]. While a lightning bolt possesses a significant amount of energy, effectively harnessing and storing it is a challenging endeavor due to the unpredictable and perilous nature of lightning [7].

Due to the nature of lightning, the impulse generator takes place as a lightning simulator in modern lightning research. This device is an electrical contraption that originates impetuous high-voltage or high-current surges [8].

The associate editor coordinating the review of this manuscript and approving it for publication was Lei Chen.

Such contrivances can be categorized as (i) Impulse Voltage generator and (ii) Impulse Current generator. Tesla coil or Jedlik's tubular voltage generator and Marx generator can be categorized as the impulse voltage generator [9]. Some impulse generator produces very high current and low voltage impulse. Such generators are called current impulse generators [10]. Other than these two types of impulse generators, a balanced impulse generator may generate high voltage and high current impulses. Tesla coil is the most economical impulse voltage generator that can act as a lightning simulator. Tesla coil is widely applied throughout basic science, medical science, and engineering science. In 1891, Nikola Tesla (1856 - 1943) invented a resonant air-core transformer named the Tesla coil. This invention has genuinely evolved the advancement of lightning research [11]. In 1892, he presented the experimental reports on a high voltage and high-frequency AC using a Tesla coil in his lecture [12].

Later, Smith experimented on the discharge of an electrified body by using a Tesla coil. The experiment was conducted using sealing wax, glass rod, and Tesla coil [13]. In 1970, Robert Golka manufactured a Tesla coil to produce artificial lightning for assessing the effects of lightning on aircraft at Wendover Air Force Base in Utah [14]. The Tesla coil, with its HV transformer, Tank capacitor or Capacitor bank, Primary coil, secondary coil, and top-load, is a marvel of electrical engineering. The efficiency of this magnificent device is highly dependent on the proper design of these elements. Moreover, the inclusion of a Spark gap serves as a protective shield against damage from high voltage, adding to the reliability and longevity of the Tesla coil.

The production of non-standard impulses by the Tesla coil or Lightning impulse in this experiment deviates from the IEEE Standard IS 2071-1 [15], [30]. While the primary side coil's shape, construction, and material are crucial factors in developing a Tesla coil, there is much confusion about how to select the appropriate primary coil for a given application. Interestingly, Sir Nicolas Tesla did not describe any specific method for selecting various shaped primary coils. This paper presents the selection criteria of the primary side coil in the Tesla coil to produce artificial lightning for the lightning energy harvester validated by the computation environment. Different shapes of primary side coil performance analyses have been conducted using the Ansys electronics environment. Various selection criteria have been proposed from those analyzed reports. A hardware model of the Tesla coil is constructed using the proper primary coil. The primary coil is selected according to this article's proposed method and equations. The method and process may help high voltage tesla coil designers to accurately distinguish each part of a tesla coil through the equations presented in this article. Presented equations are formulated according to hardware models using industrial standards, which may also help industrial tesla coil designers. This method can be utilized in wireless power transfer, high voltage testing, and various medical industries where tesla coils are used [16], [17], [18].

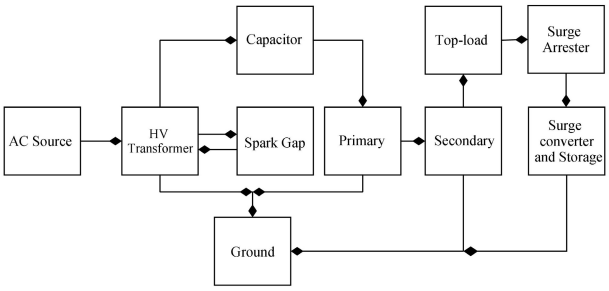

FIGURE 1. Methodology of the experiment.

II. SYSTEM METHODOLOGY

The system presented here aims to test the effectiveness of a lightning energy harvester using a Tesla coil as an artificial lightning simulator. This section details the system methodology utilized for modeling the Tesla coil lightning simulator in the context of energy storage from lightning.

Fig. 1 shows the block diagram of the system, which describes the methodology. In this system, the Tesla coil functions as a high voltage impulse generator. An aluminum rope with a nail head triggers the output spark of the Tesla coil, and a surge arrester connects the aluminum rope to a lightning energy harvester. As shown in figure 1, the AC source is used to power the high voltage transformer. Moreover, a static spark gap is used in a parallel connection to protect the transformer. The primary side LC circuit is connected in parallel with the HV transformer, then connecting the ground. The secondary coil and top-load form the secondary side LC circuit. Top-load of the Tesla coil generates a high voltage spark, which is directed by a surge arrester to the ground through a lightning energy harvester or surge converter and storage system.

Fig. 2 shows the circuit diagram, and fig. 3 shows the prototype model of the Tesla coil lightning simulator with a partial photograph of the lightning energy harvesting device. In this section, we illustrated the different parts of the system by numbers as references from figure 2 and figure 3.

(1) Power source This is a power source for the system, and we used 230 V, 50 Hz AC as power input.

(2) Transformer: A waterproof epoxy-filled 15 kV, 30 mA Neon transformer is used to produce a 15kV potential difference for the tesla coil. The dimension of the transformer is $20.3 \times 8.9 \times 10.2$ cm. The input voltage of this transformer is 220V, 50 Hz AC. This transformer has a dual output of 7.5 kV at each HT-Terminal and 30mA of current output.

(3) Transformer ground: The transformer body is connected with earthing of the mains.

(4) Spark Gap: The spark gap has been contrived to maintain the charging of the Capacitor bank. It uses the air as the conduction path between its electrodes. It produces enormous heat and noise in operation. The gap size may be adjusted according to the supply voltage [19]. Spark gaps can be classified as (i) Static spark gap, (ii) Static triggered

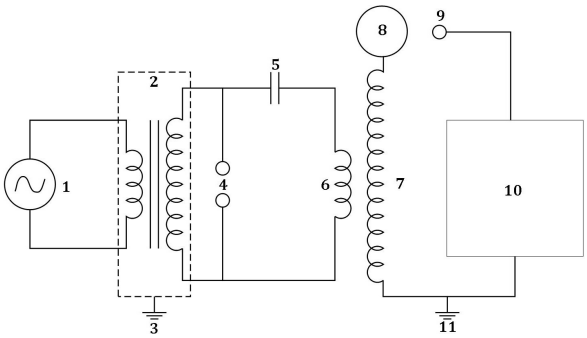

FIGURE 2. Circuit diagram of the proposed system.

FIGURE 3. Prototype of the Tesla coil lightning simulator hardware.

spark gaps, and (iii) Rotary spark gap. The spark rate of the static spark gap depends on the line frequency and can not be adjusted manually. A static spark gap is used in this system, made by two screws as electrodes [20].

(5) Capacitor bank: A capacitor bank is used to produce an immensely high resonant frequency and enhance the Tesla coil's current output. In this project, a Multi-Miniature-Capacitor (MMC) is utilized as a capacitor bank. The MMC is made up of several smaller commercial capacitors with a voltage rating of 2kV, which are connected in a series-parallel array to meet the necessary voltage, capacitance, and current requirements. Capacitor specifications are taken from datasheets and graph readouts. The different ratings of the MMC capacitor bank are measured using the following equations [21]. Capacitor bank voltage rating can be determined from,

$$V_{tc} = V_{dc} \times N_{cs} \tag{1}$$

where, V_{tc} = Capacitor bank voltage rating, V_{dc} = DC voltage rating and N_{cs} = No. of capacitors in series.

And Capacitor bank capacitance can be determined from,

$$C_{tc} = \frac{C_s \times N_{cp}}{N_{cs}} \tag{2}$$

where, C_{tc} = Capacitor bank capacitance, C_s = Single capacitor capacitance, N_{cp} = No. of capacitors in parallel and N_{cs} = No. of capacitors in series.

(6) Primary side coil: The primary side coil and the main Capacitor bank form the primary resonant (LC) circuit. A Tesla Coil must have identical primary and secondary resonant frequencies for proper operation. Primary side resonant frequency can be calculated using the following equation [22].

$$F_{r_p} = \frac{1}{2\pi\sqrt{L_p C_{tc}}} \tag{3}$$

where, F_{r_p} = Resonant frequency of primary side, L_p = Inductance of primary coil, C_{tc} = Capacitor bank capacitance.

(7) Secondary side coil: Sir Nikola Tesla did not show the construction of a secondary side coil of Tesla coil [23]. James B. Kelley and Lee Dunbar demonstrated the construction of a secondary side coil in their article [24]. But, their article lacks the adequate selection criteria for the primary side coil, which is crucial in the design of the system. The primary responsibility of generating high voltages lies with the secondary side coil, which can be divided into four key areas: the form, the wire, the insulation, and the connections. The inductance of the Secondary coil can be calculated through the following equation [25].

$$L_s = \frac{N_s^2 R_s^2}{9R_s + 10H_s} \tag{4}$$

where, L_s = Inductance of the secondary coil,N_s = Number of turns at secondary coil, R_s = Radius of the Secondary coil, H_s = Height of the secondary coil.

(8) Top-load: The top-load or discharge terminal serves a dual purpose. Firstly, it acts as a capacitor load, and secondly, it functions as the output terminal for streamer discharges. In this project, the capacitance of a spherical top-load can be calculated using equation no. 5 [26].

$$C_{tl} = \frac{k}{k_e} \times R_{tl} \tag{5}$$

where, C_{tl} = Capacitance of the Top-load, κ = Dielectric constant, R_{tl} = Radius of the Top-load and κ_e = Coulomb constant ($= \frac{1}{4\pi\epsilon_0} = 8.99 \times 10^9$). The secondary resonant (LC) circuit is formed by the secondary side coil and the top-load. Secondary side resonant frequency can be calculated using the following equation [27].

$$F_{r_s} = \frac{1}{2\pi\sqrt{L_s C_{tl}}} \tag{6}$$

where, F_{r_s} = Resonant frequency of secondary side, L_s = Inductance of secondary coil, C_{tl} = Top-load capacitance.

(9) Surge arrester: In 1872, C. W. Siemens delved into the subject of lightning conductors and shared his experiments

TABLE 1. Parametric values of components used in Tesla coil hardware.

No.	Components	Parametric values		
		Parameters	Values	Unit
1	Source	Voltage	220	V
		Frequency	50	Hz
2	Transformer	Voltage	15	kV
		Current	0.3	mA
3	Spark gap	Length	1.5	mm
4	Capacitor bank	Capacitance	3.35E-8	F
		Voltage	14	kV
5	Primary coil	Length	3.369	m
		Inductance	8.233E-6	H
6	Secondary coil	Length	283	m
		Inductance	0.0133	H
		Self capacitance	7.984E-12	F
7	Top load	Capacitance	4.264E-12	F
8	Surge arrester	Diameter	10	mm
9	Ground	Diameter	10	mm

and discoveries on the use of pointed metal as a conductor [28], [29]. In this article, a hardware model is proposed that involves attaching a pointed aluminum rope to a surge arrester. This rope is used to trigger a spark in a Tesla coil and then direct the resulting discharge to the ground through energy harvester and storage devices. The surge arrester is constructed from a Cadmium copper alloy containing about 98% copper, 1% cadmium, and 1% other materials.

(10) Surge energy harvester: Safety gap, air-core, and iron core transformer, surge gap, converter, and supercapacitors are used in high voltage surge energy harvester in a special arrangement to convert high voltage surge into a storable form of energy and to store it [30], [31].

(11) Ground: Ground rod and opposite terminal of Tesla secondary side are connected with the ground.

III. SELECTION OF PRIMARY COIL

A typical Tesla coil consists of two stages of voltage amplification. The first stage is an iron-core transformer that increases the line voltage to a higher level due to its high impedance. The second stage is a resonant air-core transformer that can further boost the voltage by more than ten times [32]. Also, the yield is at a frequency substantially higher than AC mains. The primary side coil performs a paramount role in constructing a resonant transformer. It forms the primary LC circuit along with the Capacitor bank. Three types of primary coil available may be used in the primary side LC circuit. These are (i) Flat spiral coil, (ii) Helical coil, and (iii) Inverse conical coil. However, proper conductor selection to construct the primary coil is primarily mandatory. The essential and most critical criteria are discussed in the following subsections.

A. CONDUCTOR SELECTION

Designing and assembling the primary coil presents a daunting challenge for a Tesla generator that seeks both balance and effectiveness. When the capacitor bank pulse oscillates with a potent RF current, it unleashes immense energy that manifests the infamous ''skin effect'' in the conductor, causing further complications.

(a) Silver-plated conductor: Silver-plated smooth flat strap conductor is the best conductor for this type of high energy. This type of conductor may deliver very high power to the secondary coil. However, the only problem is that sometimes this type of conductor may cause the corona effect [33]. Turn spacing should be calculated accurately to resolve this problem.

(b) Copper tube: The most used conductor for the primary side of the Tesla coil is thin wall copper tubing. Moreover, this type of copper tube has many advantages. The thin wall tubing is a magnificent conductor to carry the energy of the tank circuit. Also, the copper tube is available commercially with a variety of diameters. The smooth rounded surface helps to reduce corona loss [34]. A copper tube is used in this project for constructing the primary coil.

(c) Litz wire: Heavy Litz wire also works well as the primary coil. This type of wire is a multistrand cable used to transmit high-frequency alternating current. Using this type of wire can minimize skin effect and proximity effect losses that occur at high frequencies [35].

(d) Solid wire: Solid wire, braided strap wire, and stranded wire are not suitable for use as the primary coil in a high-frequency Tesla transformer. These types of wires can result in significant losses due to skin effect, proximity effect, and corona losses [36].

B. FLAT SPIRAL COIL

A flat spiral coil is an air-core inductor usually incorporated in the primary side of a Tesla coil [36]. The skin depth of a flat spiral coil may be formulated the following way.

If N_p is the number of turns in the coil, R_p is the average radius of coil turns, and C_p is the thickness of the coil, then inductance (L_{fsc}) of the flat spiral primary coil can be formulated using Wheeler's spiral equation [37]. Moreover, the reactance (X_{fsc}) of the coil is calculated to formulate conductance (σ_{fsc}) using $f = 50$Hz as the frequency of input power.

The inductance and reactance of the flat spiral coil may be calculated using the following equations [37].

$$L_{fsc} = \frac{N_p^2 R_p^2}{8R_p + 11C_p} \tag{7}$$

And,

$$X_{fsc} = 2\pi f L_{fsc} \tag{8}$$

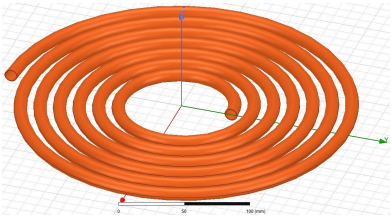

FIGURE 4. Flat spiral coil modeled in Ansys environment.

Using equation 7 and 8, we can formulate conductance in terms of physical properties of coil as,

$$\sigma_{fsc} = \frac{1}{X_{fsc}} \tag{9}$$

$$= \frac{8R_p + 11C_p}{2\pi f N_p^2 R_p^2} \tag{10}$$

And skin depth (δ_{fsc}) of the copper coil can be formulated using equation 10 as,

$$\delta_{fsc} = \sqrt{\frac{\rho}{2\pi f \mu \sigma_{fsc}}} \tag{11}$$

$$= \frac{0.12\, N_p R_p}{\sqrt{8R_p + 11C_p}} \tag{12}$$

where, ρ = Resistivity of the coil material and μ = Permeability of the coil material.

C. HELICAL COIL

A helical coil is a center line-shaped helix. One complete turn of the helix is familiar as helix pitch. A multi-layer helical coil may be catastrophic to use. The skin depth of the helical coil may be formulated following way.

If N_p is the number of turns in the coil, R_p is the radius of the coil, and H_p is the height of the coil, then inductance (L_{hc}) of the helical coil can be formulated using Wheeler's spiral equation [37]. Moreover, reactance (X_{hc}) is calculated using $f = 50$Hz as the frequency of input power to formulate conductance (σ_{hc}) of the helical type primary coil. The inductance and reactance of the helical coil may be calculated using the following equations [37].

$$L_{hc} = \frac{N_p^2 R_p^2}{9R_p + 10H_p} \tag{13}$$

And,

$$X_{hc} = 2\pi f L_{hc} \tag{14}$$

Using equation 13 and 14, we can formulate conductance in terms of physical properties of the coil as follows.

$$\sigma_{hc} = \frac{1}{X_{hc}} \tag{15}$$

$$= \frac{9R_p + 10H_p}{2\pi f N_p^2 R_p^2} \tag{16}$$

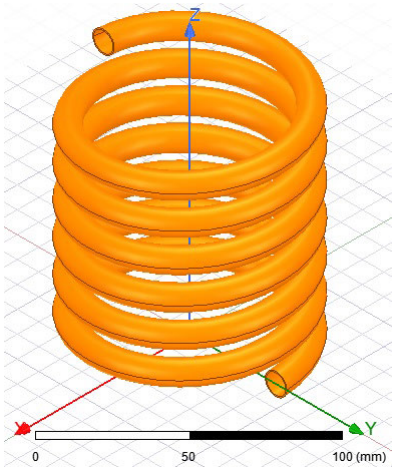

FIGURE 5. Helical coil modeled in Ansys environment.

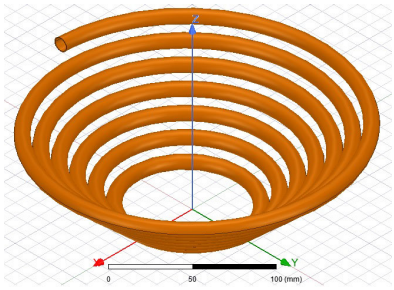

FIGURE 6. Inverse conical coil modeled in Ansys environment.

And skin depth (δ_{hc}) of the copper coil can be formulated using equation 16 as,

$$\delta_{hc} = \sqrt{\frac{\rho}{2\pi f \mu \sigma_{hc}}} \tag{17}$$

$$= \frac{0.12\, N_p R_p}{\sqrt{9R_p + 10H_p}} \tag{18}$$

where, ρ = Resistivity of the coil material and μ = Permeability of the coil material.

D. INVERSE CONICAL COIL

An inverse conical coil is a cone-shaped coil assembled inversely as a primary coil in a Tesla coil. The skin depth of the inverse conical coil may be formulated following way.

Helix factor (L_{hf}) and spiral factor (L_{sf}) of inverse conical coil are necessary to formulate inductance (L_{hc}) using Wheeler's spiral equation [37], where rise angle $\theta = 45°$. After getting the inductance and reactance (X_{hc}) of the coil, we may formulate conductance (σ_{hc}) of the inverse conical type primary coil using $f = 50$Hz as the frequency of input power. The inductance and reactance of the helical coil may

be calculated using the following equations [37].

$$L_{hf} = \frac{N_p^2 R_p^2}{9R_p + 10H_p} \tag{19}$$

$$L_{sf} = \frac{N_p^2 R_p^2}{8R_p + 11C_p} \tag{20}$$

By using equation 19 and 20 we may get,

$$L_{icc} = \sqrt{(L_{hf} sin\theta)^2 + (L_{sf} cos\theta)^2} \tag{21}$$

$$= \frac{N_p^2 R_p^2}{\sqrt{2}} \sqrt{\frac{1}{(9R_p + 10H_p)^2} + \frac{1}{(8R_p + 11C_p)^2}} \tag{22}$$

And reactance will be,

$$X_{icc} = 2\pi f L_{icc} \tag{23}$$

Using equation 22 and 23, we can formulate conductance in terms of physical properties of the coil as follows.

$$\sigma_{icc} = \frac{1}{X_{icc}} \tag{24}$$

$$= \frac{\sqrt{2}(9R_p + 10H_p)(8R_p + 11C_p)}{2\pi \mathrm{f N_p^2 R_p^2} \sqrt{(9\mathrm{R_p} + 10\mathrm{H_p})^2 + (8\mathrm{R_p} + 11\mathrm{C_p})^2}} \tag{25}$$

$$= \frac{0.0045(9R_p + 10H_p)(8R_p + 11C_p)}{N_p^2 \mathrm{R_p^2} \sqrt{(9\mathrm{R_p} + 10\mathrm{H_p})^2 + (8\mathrm{R_p} + 11\mathrm{C_p})^2}} \tag{26}$$

And skin depth (δ_{icc}) of the copper coil can be formulated using equation 26 as,

$$\delta_{icc} = \sqrt{\frac{\rho}{2\pi f \mu \sigma_{icc}}} \tag{27}$$

$$= 0.097 N_p R_p \sqrt{\frac{\sqrt{(9\mathrm{R_p} + 10\mathrm{H_p})^2 + (8\mathrm{R_p} + 11\mathrm{C_p})^2}}{(9R_p + 10H_p)(8R_p + 11C_p)}} \tag{28}$$

where, ρ = Resistivity of the coil material and μ = Permeability of the coil material.

E. PRIMARY CAPACITOR, SECONDARY COIL, AND TOP-LOAD

The skin depth of the primary coil can be fomulated from the properties of primary side capacitor, secondary coil and top load. From equation 3 and 6, we may get the inductance (L_p) of primary coil in terms of primary capacitor (capacitor bank), secondary coil and secondary capacitor (Top-load). So, it may be written using equation 2, 4 and 5 as,

$$L_p = \frac{L_s \times C_{tl}}{C_{tc}} \tag{29}$$

$$= \frac{4\pi \epsilon_0 k R_{tl} N_{cs} N_s{}^2 R_s{}^2}{C_s N_{cp}(9R_s + 10H_s)} \tag{30}$$

And,

$$X_p = 2\pi f L_p \tag{31}$$

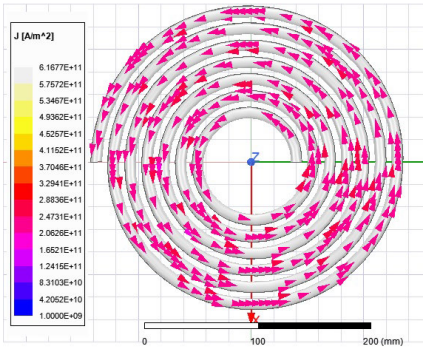

FIGURE 7. Current density vector of flat spiral coil.

Using equation 30 and 31, we can formulate conductance in terms of physical properties of primary capacitor (Capacitor bank), secondary coil and secondary capacitor (Top-load) coil as,

$$\sigma_p = \frac{1}{X_p} \tag{32}$$

$$= \frac{8\pi^2 f \epsilon_0 k R_{tl} N_{cs} N_s{}^2 R_s{}^2}{C_s N_{cp}(9R_s + 10H_s)} \tag{33}$$

And skin depth (δ_p) of the copper coil can be formulated using equation 33 as,

$$\delta_p = \sqrt{\frac{\rho}{2\pi f \mu \sigma_p}} \tag{34}$$

$$= 35 N_s R_s \sqrt{\frac{R_{tl} N_{cs}}{C_s N_{cp}(9R_s + 10H_s)}} \tag{35}$$

where, ρ = Resistivity of the coil material and μ = Permeability of the coil material.

IV. RESULT AND DISCUSSIONS

The primary coil of the Tesla coil is necessary to design to handle very high voltage and current. The proper primary coil design makes the Tesla coil well balanced and efficient. This section presents the response of different types of primary coil simulated and measured in the Ansys electronics environment. Different responses, i.e., current density, ohmic loss, electric field strength, charge density, and energy content, are measured and analyzed here. Input voltage and frequency to these coils are 15 kV and 50 Hz, respectively.

A. CURRENT DENSITY

The design of the primary side coil for a Tesla coil is heavily influenced by current density, as it has a significant impact on circuit behavior. The current density can be calculated by the physical properties of the primary coil using the designed current level [38]. Figure 7, figure 8, and figure 9 show the current density vector across flat spiral type, helical, and inverse conical coils. As shown in figure 8, the Current density vector direction of the flat spiral coil is anti-clockwise with a magnitude of approximately 1.2E+11 A/m^2 to 3.3E+11 A/m^2.

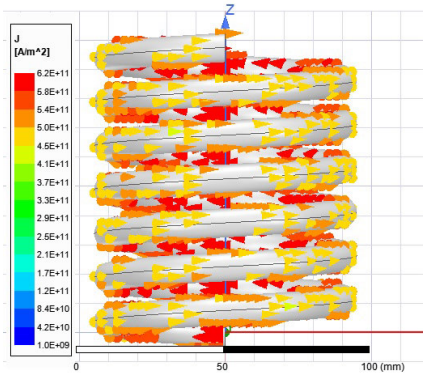

FIGURE 8. Current density vector of helical coil.

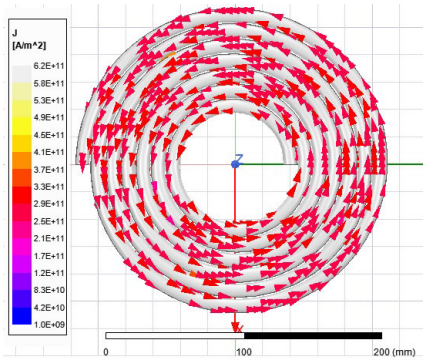

FIGURE 9. Current density vector of inverse conical coil.

Figures 9 and 10 demonstrate that the direction of the current density vector in both the helical coil and the inverse conical coil is anti-clockwise. However, they have a large difference in the magnitude range. Inverse conical coil has an approximate magnitude range of 2.1E+11 A/m^2 to 4.1E+11 A/m^2 and helical coil has an approximate magnitude range of 4.5E+11 A/m^2 to 6.2E+11 A/m^2. Some properties of a copper conductor may change due to excessive current density as it helps to raise the temperature and skin effect of the conductor. The observation shows that the current density magnitude is excessively high in the helical coil, moderately high in the inverse conical coil, and comparatively low in the flat spiral coil. Therefore, it can be said that the helical coil is not efficient as it has a relatively very high current density. This type of primary coil can produce very high power. However, in the long run, it can degrade the efficiency of the Tesla coil. Sometimes it can be catastrophic for the system.

B. OHMIC LOSS

Ohmic loss is the next fundamental property to pay attention to while designing a primary coil. Ohmic loss is caused by influences between electrons and the atomic ions in the copper tube. It depends directly on the current density, the temperature rise, contact resistances, and supply frequency to the conductor [39].

TABLE 2. Parametric response of current density in various coil type.

No.	Coil type	Current density (A/m^2)	
		Max	Min
1	Flat spiral coil	3.3E+11	1.2E+10
2	Helical coil	6.2E+11	4.5E+11
3	Inverse conical coil	4.1E+11	2.1E+11

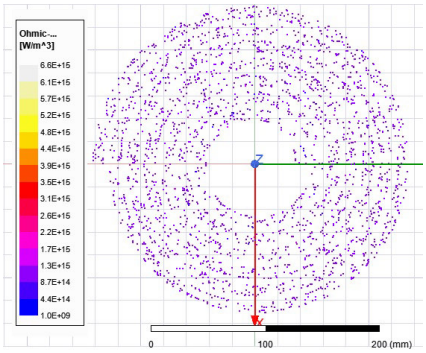

FIGURE 10. Ohmic loss of flat spiral coil.

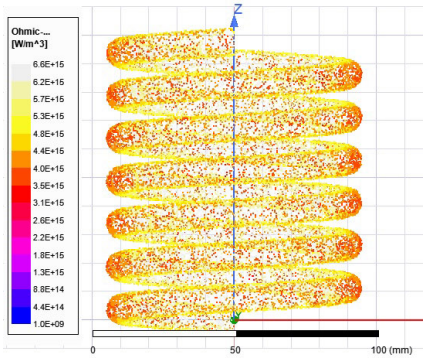

FIGURE 11. Ohmic loss of helical coil.

The proximity effect and skin effect increase in high frequency, and it causes the current to be non-uniformly distributed across the conductor. This non-uniform distribution of current in the conductor increases its active resistance. Moreover, this tendency in the high-frequency system is the cause of very high power loss and system inefficiency. Imprecise contact also increases very high ohmic loss and produces internal surges between connections.

Figure 10, figure 11, and figure 12 show the ohmic loss in flat spiral type, helical, and inverse conical coils. The dependency of ohmic loss on current density can be adequately seen from these responses. As shown in figure 10, ohmic loss in the flat spiral coil is approximately 4.4E+14 W/m^3 to 1.3E+15 W/m^3.

Moreover, as shown in Figures 11 and 12, the inverse conical coil has an approximate ohmic loss of 8.8E+14 W/m^3 to 2.6E+15 W/m^3, and the helical coil has an approximate ohmic of 3.1E+15 W/m^3 to 5.7E+15 W/m^3.

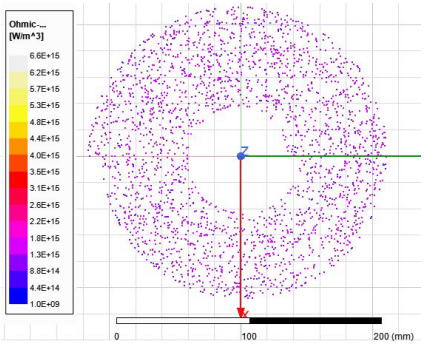

FIGURE 12. Ohmic loss of inverse conical coil.

TABLE 3. Parametric response of Ohmic loss in various coil type.

No.	Coil type	Ohmic loss (W/m^3)	
		Max	Min
1	Flat spiral coil	1.3E+15	4.4E+14
2	Helical coil	5.7E+15	3.1E+15
3	Inverse conical coil	2.6E+15	8.8E+14

C. ELECTRIC FIELD STRENGTH

Electric field strength refers to the intensity of an electric field at a specific point on the path of a conductor. This field influences other nearby charged objects. The electric field strength at the primary coil conductor's surface is a crucial factor in determining the appropriate primary coil type.

The primary coil may experience the corona effect due to its high electric field strength. The correlation between the maximum electric field strength at the primary coil and its critical electric field strength determines the direction of the electric field strength in the primary coil. The maximum electric field strength on the surface of the primary coil conductors is influenced by factors such as the maximum input voltage, coil diameter, bundle configuration, and turn-spacing.

Figures 13, 14, and 15 depict the electric field strength for the flat spiral, helical, and inverse conical coils, respectively. It is important to note that the electric field strength at the surface of the conductors should not be too high as it can increase the likelihood of the corona effect.

As shown in figure 13, the Electric field strength in the flat spiral coil is approximately 26.4 V/cm to 50.3 V/cm. Moreover, as shown in Figures 14 and 15, the helical coil has a relative Electric field strength of 68.4 V/cm to 121.1 V/cm, and the inverse conical coil has relative Electric field strength of 40.1 V/cm to 68.6 V/cm.

D. CHARGE DENSITY

For any electric field, the flow of charge is always significant. Also, such fields may have an accumulation of electric charges. Thus charge density computation is significant to calculate for different purposes. Such charge density has to be calculated based on the surface area. Figure 16, figure 17, and figure 18 show the Charge Density in flat spiral type coil, helical type coil, and inverse conical coil. The presence of electric charges is the origin of the electric field, which

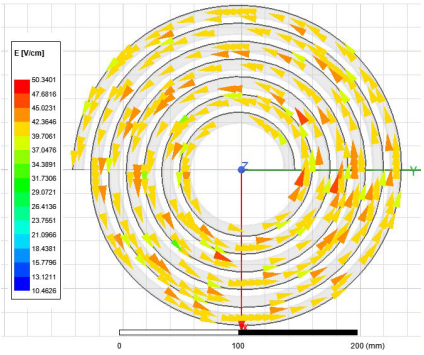

FIGURE 13. Electric field strength of flat spiral coil.

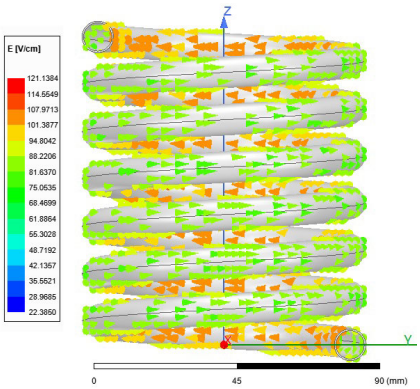

FIGURE 14. Electric field strength of helical coil.

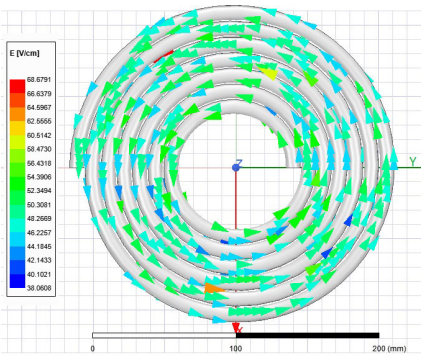

FIGURE 15. Electric field strength of inverse conical coil.

TABLE 4. Parametric response of Electric field strength in various coil type.

No.	Coil type	Electric field strength (V/cm)	
		Max	Min
1	Flat spiral coil	50.3	26.4
2	Helical coil	121.1	68.4
3	Inverse conical coil	68.6	40.1

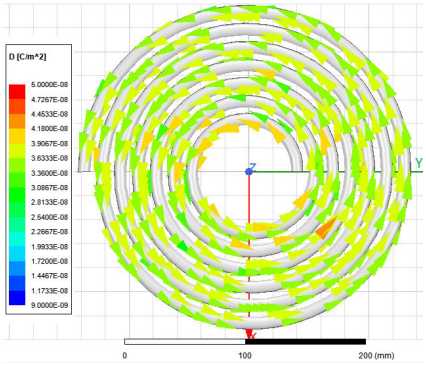

FIGURE 16. Charge Density of flat spiral coil.

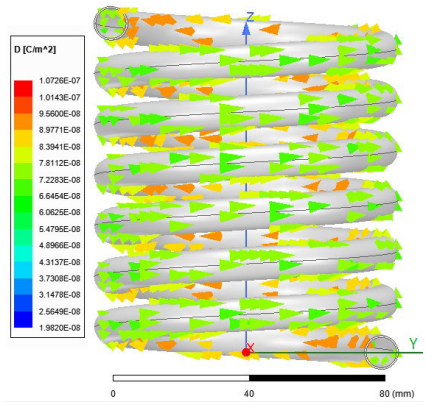

FIGURE 17. Charge Density of helical coil.

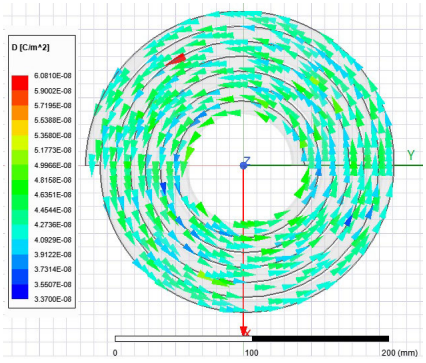

FIGURE 18. Charge Density of inverse conical coil.

means that the electric field at any given point in space can be mathematically linked to the charges that exist there.

As shown in figure 16, Charge Density in the flat spiral coil is approximately 2.3E-08 C/m^2 to 4.7E-08 C/m^2. And as shown in figure 17 and 18, helical coil has an approximate Charge Density of 5.5E-08 C/m^2 to 1.1E-07 C/m^2 and inverse conical coil has approximate Charge Density of 3.3E-08 C/m^2 to 6.1E-08 C/m^2.

TABLE 5. Parametric response of charge density in various coil type.

No.	Coil type	Charge Density (C/m^2)	
		Max	Min
1	Flat spiral coil	4.7E-08	2.3E-08
2	Helical coil	1.1E-07	5.5E-08
3	Inverse conical coil	6.1E-08	3.3E-08

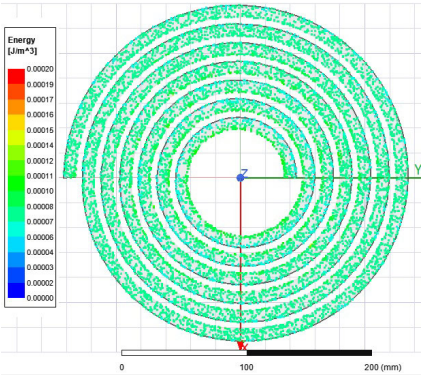

FIGURE 19. Energy content in flat spiral coil.

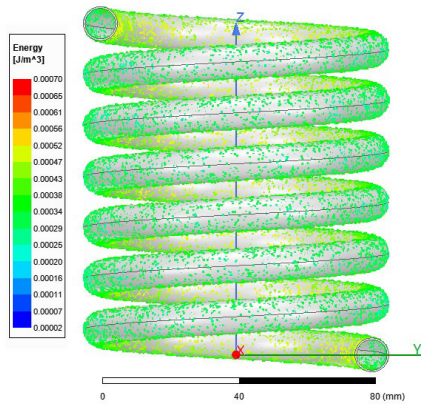

FIGURE 20. Energy content in helical coil.

E. ENERGY CONTENT

The energy content of a system or region of space per unit volume refers to the amount of energy stored. Though commonly referred to as energy per unit mass, the accurate term for this is specific energy.

Figure 19, figure 20, and figure 21 show the Energy Density in flat spiral type, helical type, and inverse conical coils. It is shown in figure 19 the Energy content in the flat spiral coil is approximately 0.00015 J/m^3 to 0.00003 J/m^3. Moreover, as shown in Figures 20 and 21, the helical coil has an approximate energy content of 0.00061 J/m^3 to 0.00025 J/m^3, and the inverse conical coil has an approximate energy content of 0.00018 J/m^3 to 0.00011 J/m^3.

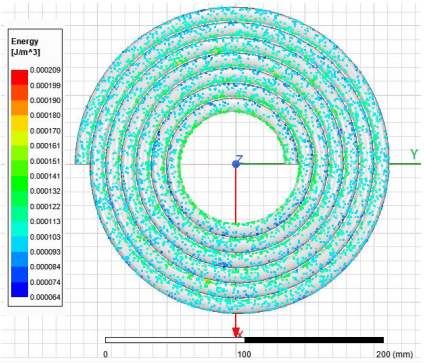

FIGURE 21. Energy content in inverse conical coil.

TABLE 6. Parametric response of Energy content in various coil type.

No.	Coil type	Energy content (J/m^3)	
		Max	Min
1	Flat spiral coil	0.00015	0.00003
2	Helical coil	0.00061	0.00025
3	Inverse conical coil	0.00018	0.00011

F. SKIN DEPTH

When an electric charge is applied to a hollow copper tube, it creates a distribution of charges on the outer surface of the tube. This distribution of charges generates an electric field outside the conductor.

This electric field allows charges to flow onto the conductor, producing an electric field opposite to the charge inside the hollow conductor.Furthermore, according to Gauss's law and symmetry, the electric field inside the shell is zero because the Gaussian surface encloses no charge, as all of the charges lie on the shell. The skin effect of the conductor is closely linked to this phenomenon. Due to the low skin effect, a hollow conductor is always preferable. The parameters mentioned here are directly or indirectly influenced by the skin depth of the conductor. So, Proper calculation of the skin depth of the conductor can give an approximate idea for mentioned parameter responses in a selected conductor. The skin depth of conductors can be formulated using equation 12, equation 18, equation 28, and equation 35. According to calculated skin depth, a flat spiral coil has the most profound skin depth among all shapes. The skin depth generated in the inverse conical coil is also considerable. However, in the helical coil, the skin depth is shallow.

V. HARDWARE VALIDATION

All the parameters observed in the ANSYS environment are validated using the hardware setup of the Tesla coil. The experimented data are tabulated in table 7. Table 7 shows the output response of tesla coil hardware. Some parameters are calculated using the respective equation using accurate data observed from the hardware setup. As shown in Table 7, the hardware setup of the tesla coil produced

TABLE 7. Parametric response of hardware setup.

No.	Parameters	Hardware response	
		Values	Unit
1	Output spark current	1.154	A
2	Output spark voltage	116	kV
3	Output spark frequency	667	KHz
4	Current density at primary coil	4.932E+10	A/m^2
5	Ohmic loss at primary coil	8.261E+14	W/m^3
6	Electric field strength at primary coil	27.403	V/cm
7	Charge density at primary coil	3.728E-08	C/m^2
8	Energy content at primary coil	0.000116	J/m^3
9	Resonant frequency at primary side	668	KHz
10	Output spark length	43.2	cm

almost 17 inches of the spark of approximate 116 kV, 1.15A, and 667KHz impulse properties. The resonance frequency produced in the primary coil is 668 kHz. Primary coil data are calculated at the end of the first turn using various hardware parameters. It is observed from the hardware data that the hardware response lies between the maximum and minimum boundaries observed in the computing environment.

Current density, ohmic loss, electric field strength, charge density, and energy content at the primary coil are calculated from observed data of tesla coil hardware. It is observed that the current density in the endpoint of the first turn is 4.932E+10 A/m^2 which lies between the maximum (3.3E+11) and minimum (1.2E+10) values of current density observed in the ANSYS environment. The ohmic loss in the end point of primary coil hardware first turn is observed at 8.261E+14 W/m^3, where the maximum-minimum boundary observed in ANSYS results are 1.3E+15 and 4.4E+14. Electric field strength observed in tesla transformer primary coil hardware is 27.403 V/cm which also lies between the min-max (26.4-50.3) boundary observed in the simulation environment. The charge density observed in the tesla coil hardware setup is 3.728E-08 C/m^2. Simulation data of charge density shows the max-min boundary of 4.7E-08 to 2.3E-08. In the first turn of the primary coil hardware endpoint, energy content data shows the value of 0.000116 J/m^3, which lies between max-min (0.00015 - 0.00003) data recorded from the ANSYS environment.

VI. CONCLUSION

Sir Nicolas Tesla blueprinted the Tesla coil to generate an enormous voltage, accompanied by enormous frequency. So, it can be inefficient and catastrophic if any part is not constructed accurately. The first voltage step-up happens in the HV transformer. The second voltage step-up happens in the primary coil. As a result, each turn of the primary coil experiences a high voltage distribution. The next step-up occurs after the coupling of the primary and secondary

coils. Maintaining the voltage distribution within the primary coil below the tolerance level of the secondary coil is crucial to prevent potential damage to the coil and internal surges.

It is observed from the analyzed results that the average current density of a flat spiral coil is 1.38 times lesser than the inverse conical coil and 2.38 times lesser than the helical coil. The average ohmic loss of a flat spiral coil is two times lesser than the inverse conical coil and 5.06 times lesser than the helical coil. A flat spiral coil's average electric field strength is 1.42 times lesser than the inverse conical coil and 2.47 times lesser than the helical coil. The average charge density of a flat spiral coil is 1.34 times lesser than the inverse conical coil and 2.36 times lesser than the helical coil. The average energy content of a flat spiral coil is 1.61 times lesser than the inverse conical coil and 4.78 times lesser than the helical coil. Due to these properties, the possibilities of corona effect, strike back, temperature rise, and noise can be minimized dramatically in a flat spiral type primary coil. Using this type of primary coil may improve the skin effect and efficiency, making it a suitable choice for low-power lightning simulator prototype testing for energy storage devices.

The lightning energy harvester is a device that extricates the impulse energy using an impulse island controller and transforms the extricated energy through a multi-level transformation system. The impulse island controller is used as an object where output surge from the tesla coil is applied. It is sometimes necessary to apply a continuous impulse strike to test the efficacy of the lightning energy harvester. Not only that, but sometimes it is also necessary to increase the output power to make a different observation. In this case, the temperature and skin effect are essential in the tesla transformer primary coil.

After analyzing the data and system response, it has been determined that using a flat spiral coil as the primary coil in a Tesla coil can provide a range of benefits. This type of coil can handle extremely high voltage and frequency, making it ideal for applications that require a high level of power output.

Moreover, the experiment has shown that a flat spiral coil can produce a resonant frequency that is better than other types of coils, such as helical and inverse conical coils, when the same amount of input power is used. Additionally, this type of coil does not heat up as quickly as other coils, which provides more room for input power increment and ensures a safer and more efficient operation.

A flat spiral coil offers a notable advantage of having lower strike-back possibilities compared to other coil types, such as helical or inverse conical coils. This makes it an ideal choice for an artificial lightning simulator that requires adjustments for more power.

Overall, the flat spiral coil offers a unique combination of high-power input, high-frequency output, and increased safety, making it the best choice for applications that require high power and reliable performance.

NOMENCLATURE

C_{tc}=Capacitor bank capacitance
C_{tl}=Capacitance of top-load
C_p=Thickness of the coil
C_s=Single capacitor capacitance
δ_p=Skin depth of primary coil conductor
δ_{fsc}=Skin depth of flat spiral primary coil conductor
δ_{hc}=Skin depth of helical coil conductor
δ_{icc}=Skin depth of inverse conical coil conductor
ϵ_0=Absolute dielectric permittivity of vacuum
f=Frequency in Hz
F_{r_p}=Resonant frequency of primary side
F_{r_s}=Resonant frequency of secondery side
H_p=Height of the primary coil
H_s=Height of the secondery coil
κ=Dielectric constant
κ_e=Coulomb constant
L_p=Inductance of primary coil
L_{fsc}=Inductance of flat spiral primary coil
L_{hc}=Inductance of helical primary coil
L_{icc}=Inductance of inverse conical primary coil
L_{hf}=Helix factor of inverse conical coil
L_s=Inductance of secondery coil
L_{sf}=Spiral factor of inverse conical coil
μ=Permeability of coil material
N_{cp}=No. of capacitor in parallel
N_{cs}=No. of capacitor in series
N_p=No. of turns in primary coil
N_s=No. of turns in secondery coil
L_p=Inductance of primary coil
R_p=Average radius of coil turns
R_{tl}=Radius of top-load
R_s=Radius of the secondery coil
ρ=Resistivity of coil material
σ_p=Conductance of primary coil
σ_{fsc}=Conductance of flat spiral primary coil
σ_{hc}=Conductance of helical primary coil
σ_{icc}=Conductance of inverse conical primary coil
θ=Rise angle of inverse conical coil
V_{tc}=Capacitor bank voltage rating
V_{dc}=DC Voltage rating
X_p=Reactance of primary coil
X_{fsc}=Reactance of flat spiral primary coil
X_{hc}=Reactance of helical primary coil
X_{icc}=Reactance of inverse conical primary coil

ACKNOWLEDGMENT

The authors would like to thank Bhagyashree Jana from the Mathematics Department, K.A.B.V. High School for her assistance in various aspects of the analysis and experiment.

REFERENCES

[1] W. Qi, L. Xiaoming, Y. Tian, and L. Longnv, "Research on transient insulation numerical analysis method of circuit breaker in GIS under lightning impulse voltage," in *Proc. IET Int. Conf. AC DC Power Transmiss.*, 2019, pp. 3320–3324.

[2] X. Fan, Y. Zhang, P. R. Krehbiel, Y. Zhang, D. Zheng, W. Yao, L. Xu, H. Liu, and W. Lyu, "Application of ensemble empirical mode decomposition in low-frequency lightning electric field signal analysis and lightning location," *IEEE Trans. Geosci. Remote Sens.*, vol. 59, no. 1, pp. 86–100, Jan. 2021.

[3] R. Bhattarai, N. Harid, H. Griffiths, and A. Haddad, "Application of surge arresters for lightning protection of 33kV," in *Proc. Int. Conf. Electr. Distrib.*, 2009, pp. 8–11.

[4] A. A. Potapov and V. A. Cerman, "Features of multi-fractal structure of high-altitude lightning discharges in the ionosphere: Elves, jets, sprites," *J. Eng.*, vol. 2019, no. 20, pp. 6781–6783, Oct. 2019.

[5] R. Hasbrouck, "Mitigating lightning hazards," *Sci. Technol. Rev.*, pp. 4–12, May 1969.

[6] V. A. Rakov, "A review of positive and bipolar lightning discharges," *Bull. Amer. Meteorological Soc.*, vol. 84, no. 6, pp. 767–776, Jun. 2003.

[7] D. M. Lal and S. D. Pawar, "Relationship between rainfall and lightning over central Indian region in monsoon and premonsoon seasons," *Atmos. Res.*, vol. 92, no. 4, pp. 402–410, Jun. 2009.

[8] *Artificial Lightning*, Amer. Assoc. Advancement Sci., Washington, DC, USA, vol. 69, 1929.

[9] N. Khan, N. Mariun, I. Aris, and J. Yeak, "Laser-triggered lightning discharge," *New J. Phys.*, vol. 4, p. 61, Aug. 2002.

[10] J. H. Chiles and W. L. Teague, "The impulse generator and its uses," *Electr. Eng.*, vol. 71, no. 8, p. 690, Aug. 1952.

[11] C. M. Jarvis, "Nikola Tesla and the induction motor," *Phys. Educ.*, vol. 5, no. 5, pp. 280–287, Sep. 1970.

[12] N. Tesla, "Lecture of Nikola Tesla," *J. IEE*, vol. 21, no. 97, pp. 52–162, 1892.

[13] F. J. Smith, "Discharge of an electrified body by means of the Tesla spark," *Nature*, vol. 54, no. 1396, p. 296, Jul. 1896.

[14] X. Qie, R. Jiang, and P. Laroche, "Triggering lightning experiments: An effective approach to the research of lightning physics," *J. Aerosp. Lab*, vol. 35, pp. 1–13, Dec. 1978.

[15] T. Takahashi, "Riming electrification as a charge generation mechanism in thunderstorms," *J. Atmos. Sci.*, vol. 35, no. 8, pp. 1536–1548, Aug. 1978.

[16] Z. Yu, M. Stjernstrom, and F. Laurell, "High aspect ratio microchannels fabricated in fused silica holllow fibres using a Tesla coil," *Appl. Phys. Lett.*, vol. 20, no. 7, 1972, pp. 239–241.

[17] W. Cao, S. Wan, S. Gu, H. Xu, J. Chen, J. Wang, and J. Lv, "Development and application of lightning flashover limited equipment for 220 kV AC transmission line," *J. Eng.*, vol. 2019, no. 16, pp. 802–805, Mar. 2019.

[18] J. Pokorny, P. Marcon, J. Janousek, T. Kriz, and P. Dohnal, "A wireless charging station for multipurpose electronic systems," in *Proc. Photon. Electromagn. Res. Symp.*, 2019, pp. 2093–2097.

[19] R. Hull, "The Tesla coil builder's guide to the Colorado springs notes of Nikola Tesla," *Tesla Coil Builders Richmond Virginia*, vol. 11, no. 1, pp. 7–18, 1993.

[20] H. Matsuzawa and S. Suganomata, "Design charts for Tesla-transformer-type relativistic electron beam generators," *Rev. Sci. Instrum.*, vol. 53, no. 5, pp. 694–696, May 1982.

[21] R. M. Hall and R. Battino, "Making an inexpensive Tesla coil from a car coil," *J. Chem. Educ.*, vol. 73, no. 8, pp. 817–818, 1996.

[22] A. Haddad and D. F. Warne, *Advances in High Voltage Engineering*, vol. 40. London, U.K.: IET Power and Energy, 2007, pp. 601–606.

[23] N. Tesla, "Means for generating electric currents," U.S. Patent 5 14 168, Feb. 6, 1894.

[24] M. Denicolai, *Tesla Transformer for Experimentation and Research*. Espoo, Finland: Helsinki Univ. Technol. 2001, p. 18.

[25] J. B. Kelley and L. Dunbar, "The Tesla coil," *Amer. J. Phys.*, vol. 20, no. 1, pp. 32–35, 1952.

[26] S. Shetty and P. Patel, "Wireless transmission of electrical energy from a Tesla coil using the principle of high voltage," *Int. J. Electr. Eng. Technol. (IJEET)*, vol. 8, no. 3, pp. 61–66, 2017.

[27] G. M. El-Aragi, "Construction and optimization of Tesla coil," *J. Phys. Astron.*, vol. 5, no. 3, p. 123, 2017.

[28] C. W. Siemens, "Lightning and lightning conductors," in *Proc. 8th Ordinary Gen. Meeting*, 1872, pp. 336–357.

[29] R. C. Scully, *A Study of the Characteristics and Various Platings on Cylindrical Electrical Conductors*. Arlington, TX, USA: Univ. Texas Arlington, 2013, pp. 5–12.

[30] S. Jana, "A system to store energy from high voltage impulse," Indian Patent Applicaion no. 31 029 953, Jul. 24, 2019.

[31] S. Jana, P. K. Biswas, and C. Sain, "Mathematical modeling of impulse island controller to safely store the energy from high-voltage lightning impulse," *Energy Storage*, vol. 4, no. 4, pp. 1–11, Aug. 2022.

[32] N. Tesla, "System of electric lighting," U.S. Patent 4 54 622, Mar. 23, 1891.

[33] J. E. Patterson and R. J. Miers, *The Thermal Conductivity of Common Tubing Materials Applied in a Solar Water Heater Collector*. Cullowhee, NC, USA: Western Carolina Univ., 2009, pp. 1–4.

[34] E. Mattsson and A.-M. Fredriksson, "Pitting corrosion in copper tubes—Cause of corrosion and counter-measures," *Brit. Corrosion J.*, vol. 3, no. 5, pp. 246–257, Sep. 1968.

[35] R. P. Wojda, "Winding resistance and power loss for inductors with litz and solid-round wires," in *Proc. IEEE Int. Power Electron. Motion Control Conf. (PEMC)*, Sep. 2016, pp. 860–865.

[36] D. B. Miron, "Chapter 9—Measurements, small antenna design," *Brit. Corrosion J.*, pp. 245–248, 2006.

[37] H. A. Wheeler, "Simple inductance formulas for radio coils," *Proc. Inst. Radio Eng.*, vol. 16, no. 10, pp. 1398–1400, Oct. 1928.

[38] A. Vallecchi, S. Chu, L. Solymar, C. J. Stevens, and E. Shamonina, "Coupling between coils in the presence of conducting medium Andrea," *IET Microw., Antennas Propag.*, vol. 13, no. 1, pp. 55–62, 2018.

[39] Y. Zhang, J. Su, L. Zheng, R. Li, L. Zhao, B. Yu, J. Cheng, B. Zeng, and X. Xu, "Analysis and elimination on common-mode interferences generated in the series-resonant converter system of high-power Tesla pulse driver," *IET Sci., Meas. Technol. Res.*, vol. 13, no. 7, pp. 949–958, 2019.

SUMAN JANA received the B.Tech. degree in electrical engineering from the West Bengal University of Technology, in 2013, the M.Tech. degree in electrical engineering with a specialization in power systems from the Maulana Abul Kalam Azad University of Technology (formerly known as WBUT), in 2016, and the Ph.D. degree in electrical and electronics engineering from the National Institute of Technology Mizoram, in 2022. During his Ph.D. degree, his research focused on extracting energy from high voltage lightning bolts. He is currently a Faculty Member with the Electrical and Electronics Engineering Department, Regent Education and Research Foundation. Prior to his current position, he worked as a Research Scientist with the Energy Department, Nil Prithibi Technology (P) Ltd. He also collaborated with several industrial startups to provide guidance on designing innovative energy devices. He has been recognized for his work through numerous awards and honors. Additionally, he serves as a reviewer for several leading journals in the field of electrical engineering and is actively involved in mentoring and guiding young researchers. He has published numerous research articles in various journals and international conferences and holds three Indian patents in the field of renewable energy. His research interests include lightning energy, solar energy, wind energy, ocean energy, other alternate renewable energy sources, energy storage systems, AI-controlled energy systems, and high voltage energy conversion.

PABITRA KUMAR BISWAS (Member, IEEE) received the B.Tech. degree in electrical engineering from the West Bengal University of Technology (WBUT), the M.E. degree in electrical engineering with power electronics and drives specialization from BESU (IIEST), West Bengal, India, and the Ph.D. degree in electrical engineering from the National Institute of Technology Durgapur, Durgapur, India. He is currently a Faculty Member with the Electrical and Electronics Engineering Department, National Institute of Technology Mizoram, Mizoram, India. During his academic career, he has guided several research scholars in their research pursuits, and several more are currently pursuing research under his guidance. He has also received several awards for his research contributions, including the Best Paper Award and Researcher Award (International Scientist Awards on Engineering, Science, and Medicine). With over 14 years of academic and research experience, he has authored several research papers in national/international conferences and journals. He has also reviewed papers in reputed international conferences and journals. He is a member of the Institute of Engineers and the International Association of Engineers. In addition, he is a fellow of the SAS Society (FSASS). His research interests include electromagnetic levitation systems, active magnetic bearing, power electronics converters, PMSM and BLDC motor drives, electric vehicles, and renewable energy.

THANIKANTI SUDHAKAR BABU (Senior Member, IEEE) received the B.Tech. degree from Jawaharlal Nehru Technological University, Ananthapur, India, in 2009, the M.Tech. degree in power electronics and industrial drives from Anna University, Chennai, India, in 2011, and the Ph.D. degree from VIT University, Vellore, India, in 2017. He worked as a Postdoctoral Researcher with the Department of Electrical Power Engineering, Institute of Power Engineering, University Tenaga Nasional (UNITEN), Malaysia. He is currently working as an Associate professor with the Department of EEE, Chaitanya Bharati Institute of Technology, Hyderabad, India. He has published more than ten research articles in various renowned international journals. His research interests include design and implementation of solar PV systems, renewable energy resources, power management for hybrid energy systems, storage systems, fuel cell technologies, electric vehicle, and smart grid. He has been acting as an Editorial Board Member and a Reviewer for various reputed journals, such as the IEEE and IEEE Access, IET, Elsevier, EPCS, and Taylor and Francis.

HASSAN HAES ALHELOU (Senior Member, IEEE) is currently a Faculty Member with Tisheen University, Lattakia, Syria. He was a Ph.D. Researcher with the Isfahan University of Technology (IUT), Isfahan, Iran. He is included in the 2018 and 2019 Publons list of the top 1% best reviewer and researchers in the field of engineering. He was a recipient of the Outstanding Reviewer Award from *Energy Conversion and Management* journal, in 2016, *ISA Transactions* journal, in 2018, *Applied Energy* journal, in 2019, and many other awards. He was a recipient of the Best Young Researcher in the Arab Student Forum Creative among 61 researchers from 16 countries at Alexandria University, Egypt, in 2011. He has published more than 30 research papers in the high quality peer-reviewed journals and international conferences. He has also performed more than 160 reviews for high prestigious journals, including IEEE TRANSACTIONS ON INDUSTRIAL INFORMATICS, IEEE TRANSACTIONS ON INDUSTRIAL ELECTRONICS, *Energy Conversion and Management*, *Applied Energy*, and *International Journal of Electrical Power & Energy Systems*. He has participated in more than 15 industrial projects. His major research interests include power systems, power system dynamics, power system operation and control, dynamic state estimation, frequency control, smart grids, micro-grids, demand response, load shedding, and power system protection.